Desalination and Water Treatment
www.deswater.com

doi: 10.5004/dwt.2019.23905

151 (2019) 82–92
May

Development of a new photocatalytic reactor built from recyclable material for the treatment of textile industry effluents

Ada A. Barbosa[a], Ramon V. S. de Aquino[a], Ana Flávia B.Oliveira[a], Renato F. Dantas[b], Josivan P. Silva[a], Marta M.M.B. Duarte[a], Otidene R.S. da Rocha[a,*]

[a]*Department of Chemical Engineering, Universidade Federal de Pernambuco -UFPE, Av. Prof. Arthur de Sá, s/n, Cidade Universitária, Recife, Brazil, Tel. +55 81 21267322; emails: otidene.rocha@ufpe.br (O.R.S. da Rocha), adabarbosa@hotmail.com (A.A. Barbosa), viniciusramon59@gmail.com (R.V.S. de Aquino), flavia.oliveira236@hotmail.com (A.F.B. Oliveira), josivan_silva@hotmail.com (J.P. Silva)*
[b]*School of Technology, Universidade Estadual de Campinas – UNICAMP, Paschoal Marmo 1888, 13484-332 Limeira, SP, Brazil, email: renatofalcaod@ft.unicamp.br*

Received 26 July 2018; Accepted 1 February 2019

ABSTRACT

The aim of this work was to test the efficiency of a new photocatalytic reactor made of recycled materials. To perform this stu dy a textile effluent was treated by different AOPs and the solar/H_2O_2/$TiO_{2suported}$ method showed the higher percentage of degradation after the reaction time. Through a factorial design, it was possible to find the more significant variable in order to reach higher percentages of degradation. The performance of the reactor with recirculation allowed obtaining degradation kinetics parameters by adjusting the removals to a second order model, with k_{dyes} = 0.175 L.mol^{-1}.s^{-1} and 90% of dye removal after 30 min for the solar/H_2O_2/$TiO_{2suported}$ system. The use of artificial neural network was proven to be efficient to predict the degradation of a real effluent, with an absolute error of 0.02266. Other parameters such as COD, apparent color and nitrate were importantly reduced after treatment. The use of the reactor made of recycled material (PET) brings economic advantages, due to the low cost of the used materials and its respective easy construction. The treatment with the new reactor is suitable for the removal of contaminants from textile effluents since it presented higher efficiency than the conventional treatment used in the textile industry under study.

Keywords: Photocatalytic reactor; Advanced oxidation processes; Recycled materials; Textile effluent

1. Introduction

Pollution and environmental destruction caused by industrialization have been causing serious problems for the environment due to the large number of effluents generated by different processes such as tanneries, textiles, pharmaceutic, pulp and paper, petrochemicals, among others. Due to the complex composition of effluents, each industrial process has specific difficulties to reach effluents disposal limits established by the current legislation [1]. The textile segment is often associated with negative environmental impacts due to the use of large quantities of dyes in the dyeing process. Therefore, the discharge of this type of wastewater impairs the quality of the aquatic environment by changing its colour and creating conditions for eutrophication, low reoxygenation and decrease in sunlight penetration [2,3].

Considering the increasing awareness and concern about the negative effects on the discharge of industrial wastewater into the environment, more restrictive legislation were adopted regarding the concentrations of pollutants in effluents. Therefore, it is necessary to develop and implement

* Corresponding author.

environmental friendly, sustainable and energy efficient technologies for the treatment process [4]. Techniques such as electrocoagulation [5,6], adsorption [7,8] and membranes [9,10] have been used in the treatment of textile effluents, however they are not able to degrade the organic contaminants, achieving only the phase-transfer [11].

Among the techniques used for the treatment of industrial effluents, the advanced oxidation processes (AOP) were increasing their importance in the last decades. AOP can reach complete or partial oxidation of organic molecules due to the formation of reactive free radical species, such as hydroxyl radicals (HO•) [12–14]. AOP are characterized by non-selectivity radicals and the use of potent oxidizing species such as H_2O_2 and semiconductors such as TiO_2 [15,16]. Many synergistic effects were reported by the combination of these species in AOP systems [17].

The most studied AOP are the Fenton reaction, photochemical and photocatalytic processes [18,19]. Photochemical processes consist of oxidizing agents decomposition into free radicals when they are exposed to radiation, as in the UV/H_2O_2 system, which H_2O_2 absorb radiation with $\lambda < 290$ nm andis broken homolytically in HO• [15,20]. In contrast, photocatalytic processes, such as UV/TiO_2 system, involve the production of radical son the catalyst surface, usually based on more complex mechanisms. TiO_2 is a semiconductor material, which absorbs energy equal to or greater than its energy band gap (3.0–3.2 eV at 25°C), thus promoting the excitation of electrons (e^-) of the valence band (VB) to the conduction band (CB), resulting in positive (h^+) hole in the valence band. This hole, when combined with oxygenated species such as water and hydroxyl groups, can generate various free radicals. TiO_2 usage appears as a new technology for environmental protection with several advantages for its use in photocatalysis such as high efficiency, low toxicity, photochemical stability, low selectivity and low cost [21–23].

The kinetic study of oxidation process of effluents is often challenging due to the lack of knowledge about all the possible reactions steps and present compounds. One of the most promising modeling techniques is the artificial neural network (ANN). ANN does not require the physical comprehension of the phenomena involved in the process, it has been applied to solve a great variety of tasks which are difficult to solve by computational programs based in more simple rules. ANN can be used as mathematical tools for non-linear problems even with multiple inputs and outputs, which make them useful to analyze compounds degradation patterns in complex chemical processes [24,25]. ANN is able to generate a proper model to describe an effluent degradation since it can be fitted to several variations on the response.

Different models of catalytic photoreactors have been used to degrade organic pollutants [26–28]. Many studies have focused on developing more efficient AOP treatment systems by adding cost savings and increasing energy efficiency through reactor design with the objective of overcoming challenges such as the uniform distribution of radiation, internal and external mass transfer (MT), catalysts surface increase, activate sites and large-scale efficiency [29,30]. Several configurations and materials have been employed, most of which are batch operated, operating in various systems such as electrocoagulation, recirculation, fixed and packed beds, nanotubes, etc. seeking to reduce MT limitations [29,31].

TiO_2 can be used in suspended powder or immobilized on a support. The use of the catalyst in powder form is very common and its dispersion in the liquid phase is usually performed by magnetic stirring [32]. The aeration of the solution is also maintained to prevent recombination of the electron/hole and favor the dispersion of the catalyst [33]. The photodegradation efficiency is proportional to the amount of TiO_2 due to the higher availability of surface area for adsorption and degradation. However, values higher than the optimum can hinder light penetration, thus reducing the efficiency of the photocatalytic process. Therefore it is important to optimize the amount of the photocatalyst applied to the system [34,35]. Alternatively, a supported photocatalystis used. This strategy has the following advantages: facilitate recovery at the end of the process and allow better handling of the catalyst [36–39]. Many attempts have been also made in the investigation of the heterogeneous applications of TiO_2 in the forms of nanotubes, support structures and surface coating [40]. However, these processes use materials with high added value as support and the present work had the motivation to construct a reactor with recycled material, with construction cost extremely low, while having efficiency in the treatment and the advantage to have supported catalyst.

The objective of this work was to develop an efficient wastewater treatment process able to treat effluents from the textile industry using a photocatalytic bench reactor made of a recyclable material of poly (terephthalate ethylene) (PET) with supported TiO_2 on aluminium (a recyclable post-consumer material) sealing loop. In addition, the work aims to evaluate the degradation kinetics of the best system from ANN modeling.

2. Methodology

2.1. Effluent characterization

The effluent samples were collected from a jeans washing factory located in the city of Toritama (Pernambuco, Brazil). They were collected at the inlet (EI) and outlet (EO) of the effluent treatment plant of the factory. The EI was collected shortly after the passage through railing. The EO was treated through the following processes: flocculation and sedimentation process. The samples were characterized in terms of pH, turbidity, conductivity, apparent colour, total dissolved solids, nitrate and chemical oxygen demand (COD) [41].

2.2. Method for impregnating and characterization TiO_2 in the aluminium ring mesh

Aluminum seals (ring) were obtained from cans of soda (a recyclable post-consumer material). The aluminum meshes were made by cutting and fitting the seals. After the cleaning process, the aluminum sealing meshes were calcined at 490°C for 26 h. In order to impregnate the aluminum seals with TiO_2 P25 Degussa, an aqueous dispersion of TiO_2 (2% w/v) at pH 2.5 was prepared according to the procedure described by Barros et al. [37]. Then, the sealing meshes were submerged in the TiO_2 dispersion for 10 s. Afterwards, the sealing meshes were dried in the stove (QUIMIS Q315M25) for 1 h at 35°C. The impregnation procedure was repeated in order to achieve the desired mass of TiO_2 on the surface

of the mesh. After the TiO_2 immobilization, the impregnated sealing rings were muffled at 490°C for 4 h.

The samples were analyzed on a SHIMADZU UV-2550 spectrophotometer in reflectance mode. They were analyzed in continuous mode, varying the wavelength from 190 to 900 nm. The Wood and Tauc method [42] was used to interpret the UV-Vis spectrum. This model divides the spectrum into three regions according to the gap.

The samples were analyzed in an XRD-6000 diffractometer from SHIMADZU, with Cu Kα radiation, 2 kVA of power, the voltage of 30 kV and 30 mA of current. Scans were performed in the range of 2θ between 20° and 80°, with a pitch of 0.02° and a velocity of 2° s^{-1}. The characteristic peaks of the materials were compared with the crystallographic charts 21-1272 and 21-1276 (International Center for Diffraction Data) and were compared with the crystallography of the aluminium seal prior to the immobilization of TiO_2.

The Fourier transform infrared spectroscopy (FTIR) analysis was performed on a Bruker Tensor 27 Spectrometer, in a range of 4,000–500 cm^{-1} with 16 scans. The attenuated total reflectance probe coupled to the spectrometer provided a resolution of 4 cm^{-1} in order to verify the availability of TiO_2 in the samples.

The morphological evaluation of the TiO_2 nanoparticles of the aluminium support after calcination and after calcination and impregnation was performed by scanning electron microscopy (SEM Tescan MIRA3).

2.3. Photocatalytic reactors

The first sets of experiments were performed in a batch photocatalytic reactor. The reactor consisted of a 68×14×26 cm of an internal chamber, internally coated by reflective metallic material and containing a UV-C lamp (ILUMISAMPA T8, 20 W) in the cover. The overall radiation intensity of the system was estimated at 7.5 $W.m^{-2}$. The container inside the box was built with a 300 mL cylindrical recycled PET container with 8.1 cm high and 8.3 cm in diameter (Fig. 1). These containers came from the bottom of a bottle of mineral water of 1.5 L. It was placed over a magnetic stirrer.

Based on preliminary experiments in the batch system described in Fig. 1(a), the creation of a recirculation system (Fig. 1(b)) was proposed. The recirculation system was assembled consisting of two parts: a reservoir containing a pump and a PET bottle connected to a second part composed of two horizontally connected cylinders.

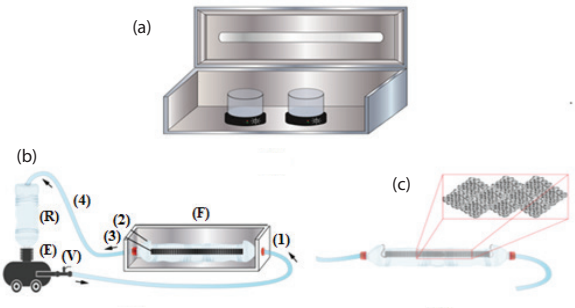

Fig. 1. Batch photocatalytic reactor built with PET bottles (a), Photocatalytic reactor with PET bottles and recirculation system containing peristaltic pump and aluminum meshes supporting TiO_2 (b), and Details of the aluminium ring mesh (c).

A washing machine electro-pump (Robertshaw, 34 W) was used in the recirculation system connected to the reservoir bottle. The bottles used were 1.5 L mineral water (Villa©). Longitudinal apertures were made in the horizontal direction of two bottles and the bottom of the third bottle in the vertical direction, as shown in Fig. 1(c). These holes were implemented along the material's surface to achieve higher light penetration rates directly into the solution. Each bottle of the reactor had approximately 160 cm^2 of surface area. Silicon connections with an internal diameter of 1.2 cm were used to connect the reservoir to the inlet and outlet of the two bottles, having the inlet tubing a flow control valve. Aluminum meshes homogeneously impregnated with TiO_2 P25 Degussa are shown in detail in Fig. 1(c). The aluminum mesh with photocatalytic material in solid form was laid submerged on the surface of the effluent during the treatments.

A tubular reactor made with two transparent beverage PET bottles (2) within a metal material reflecting chamber (F) (3).

An external reservoir (R) made with a transparent PET bottle connected to an electropump (E) and an inlet pipe for the reactor (1) and another reactor outlet pipe (4) at the top of the reservoir; The inlet pipe (1) is provided with a flow control valve.

Mesh lattice of beverage cans made of aluminum (3) made according to Fig. 3 and homogeneously impregnated with TiO_2 in solid form to be laid submerged on the surface of the solution and under the radiation during the treatment.

2.4. Analytical methodology

Samples obtained during the experiments were quantified by UV-Visible Spectroquant Pharo 300 Spectrometry (Thermo scientific). They were read at absorptions peak at a wavelength of 254 and 655 nm for the aromaticity and textile dyes, respectively. The percentage of dye removal (%) was used as a response. All samples containing TiO_2 were centrifuged at 3,500 rpm for 40 min before analysis to avoid interference of TiO_2 in the analysis. UVC light experiments were performed on a photocatalytic bench reactor shown in Fig. 1. The lamps were preheated for 30 min to stabilize the emissions. The solar experiments were conducted in Recife, Brazil (8°04′03′′S; 34°55′00′′W), during sunny days.

2.5. Preliminary tests

Preliminary tests were performed for 360 min under solar radiation or using a UVC lamp in a photocatalytic reactor, varying the amounts of H_2O_2 and TiO_2, as shown in Table 1. Prior to the experiments with radiation, all systems were under magnetic stirring in the dark for 30 min. The established time for the experiments was determined in the laboratory by previous tests on similar systems. Experiments without radiation source, TiO_2, H_2O_2 and TiO_2/H_2O_2 and direct photolysis process were also performed as blanks to evaluate the influence of radiation source, oxidants and photocatalyst. In all experiments using TiO_2 the amount used was 100 mg, based in the work of Nascimento Júnior et al. [43]. The TiO_2 P25 used was from Evonik Degussa Brasil

Table 1
AOP used in preliminary tests

UVC radiation	Solar radiation
UVC	Solar
UVC/H_2O_2	Solar/ H_2O_2
UVC/$TiO_{2suspended}$	Solar/$TiO_{2suspended}$
UVC/$TiO_{2suported}$	Solar /$TiO_{2suported}$
UVC/H_2O_2/$TiO_{2suspended}$	Solar/H_2O_2/$TiO_{2suspended}$
UVC/H_2O_2/$TiO_{2suported}$	Solar/H_2O_2/$TiO_{2suported}$

Ltda. The TiO_2 P25 Degussa is constituted by 75% of anatase and 25% of rutile and has surface area of 50 $m^2.g^{-1}$ [44]. The concentrations of H_2O_2 (50% v/v of Coremal/Pochteca) used in the degradation experiments were 2.68 and 1.88 g L^{-1} in the EI and EO, respectively, with values based on stoichiometric calculation. The sample volume was 300 mL. The used TiO_2 concentration was based on previous studies, while the amount of H_2O_2 was calculated as a function of the amount of oxygen given in the COD analysis and the obtained value was tripled. TiO_2 was recovered at the end by centrifugation. Samples were collected after 1, 5, 30, 60, 90, 120, 180, 240, 300, and 360 min.

2.6. 2^3 factorial planning for UV-Solar/H_2O_2/TiO_2 system

The factorial planning 2^3 was performed for the best system according to the preliminary tests using the batch system. The studied parameters were H_2O_2 concentration and TiO_2 dose. The center point of the 2^3 factorial planning was made in triplicate to determine the error, amounting seven experiments. The studied levels are described in Table 2.

The Solar/H_2O_2/$TiO_{2suported}$ system was chosen to perform the factorial design due to its high percentage of degradation in preliminary tests. Thus 200 mL of solution was used in each container to perform the runs. The experimental time was chosen to be 120 min.

2.7. Kinetic modeling study

From the best conditions obtained for the Solar/H_2O_2/$TiO_{2suported}$ system, the degradation kinetics was studied in the recirculation reactor. The experiment was performed in triplicate. The results obtained in the experiment were adjusted to kinetic models of zero order, pseudo-first order and second order. The kinetic constant in Eq. (1) and half-life (Eq. (2)) were calculated for the model that best describes the reaction, which in this case was the second order.

$$\frac{1}{\text{Abs}} = kt + \frac{1}{\text{Abs}\,(t=0)} \tag{1}$$

$$t_{\frac{1}{2}} = \ln\frac{2}{k} \tag{2}$$

Kinetic models using ANN were established for solar/H_2O_2/$TiO_{2suported}$ system using as response aromaticity and dye removals. The ANN was developed with the time and wavelength absorption as input variables to generate a curve of concentration over time, as used by Göb et al. [45] and Giroto et al. [46]. For this purpose, a software was created based on C# language in Unity 3D©, commonly used to develop games and apps. The ANN is composed of input, hidden and output layers with a different number of neurons. A group of procedures was set to turn the adjustment possible. The type of ANN used was 2:3:1 (2 input variables, 3 hidden layers, and 1 output variable). The training method was based on particle swarm optimization (PSO) as exposed by Kennedy and Eberhart [47], which a small disturbance was induced in the weights and biases to verify if the resultant network is a better adjustment according to the experimental data. Related to the computational effort, the training times were 86,600 s according to the requirements of enough interactions for the fit. All training was performed on a regular desktop computer.

Table 2
Variables levels of the 2^3 factorial planning

Levels	TiO_2 (mg)	H_2O_2 (g L^{-1})
–1	100	2.68
0	250	5.21
+1	400	8.04

3. Results and discussion

3.1. Characterization of aluminium ring mesh

The spectra obtained by UV-VIS diffuse reflectance analysis are shown in Fig. 2. TiO_2 P25 (Degussa) was used as a reference to verify the possible increase of the E-gap in the sample in the place that the catalyst was immobilized.

The optical band gap (E-gap) was estimated by the Wood and Tauc method [42], according to the authors the optical band gap is associated with the absorbance and energy of the photon. The values (E-gap) were calculated by extrapolating the linear region of the curve. As observed in Fig. 2, there is a slight increase in band gap when comparing TiO_2 P25 (Degussa) and TiO_2 immobilized in an aluminum seal after calcination. The sample of pure TiO_2 shows Egap of 3.03 eV while the sample immobilized in aluminium ring shad an E-gap of 3.1 eV. Probably this lower band gap may favor the degradation of the compounds when solar radiation is used.

The X-ray diffraction (XRD) spectra of TiO_2 immobilized on the aluminum seal are shown in Fig. 3. The qualitative interpretation of the compounds present in the catalysts was performed from the inorganic crystal structure database (ICSD) database: 21-1272 and 21-1276. It is possible to note the presence of the anatase and rutile phases of TiO_2, as well as the presence of the metallic aluminum substrate (sealing). Peaks at 25.53°, 37.20°, 38.6°, 48.31°, 55.00°, 62.6° and 75.06° refer to the anatase phase of TiO_2 for different crystalline planes. The rutile phase of peaks refers to 27.88°, 41.2°, 54.48°, 65.26° and 69.46°. The peaks at 43.22° and 44.84° are probably related to the presence of the aluminum metal substrate.

Fig. 4 shows the FTIR spectrums for the aluminum support, calcined, and immobilized with TiO_2 and calcined and immobilized with TiO_2 after the treatment of the effluent.

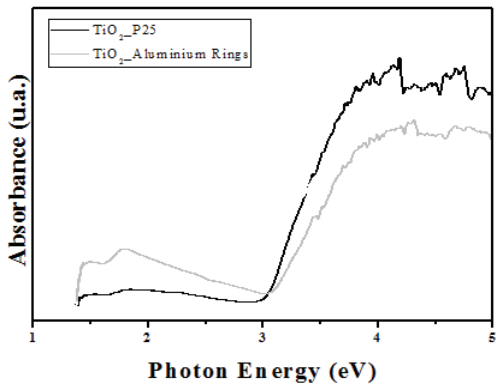

Fig. 2. Visible UV Spectra of TiO_2 and $TiO_{2Calcined}$ (aluminum rings).

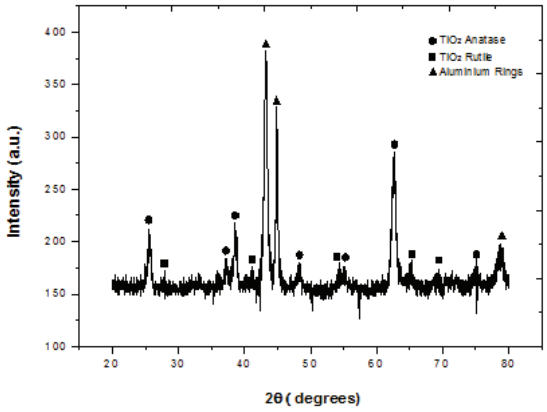

Fig. 3. Diffractogram of TiO_2 immobilized in aluminum seal.

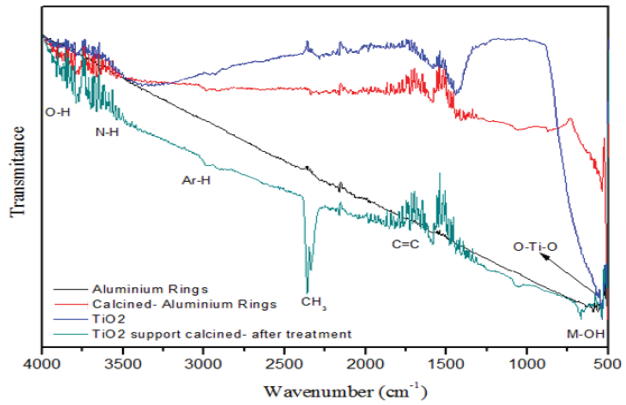

Fig. 4. FTIR analysis of aluminium supports without calcination, with calcination, calcined with immobilized TiO_2 and calcined with immobilized TiO_2 after the treatment of the textile effluent.

In the case of the support calcined and immobilized on TiO_2 after the treatment, the stretch of characteristic groups of textile dyes containing hydrogen, such as the hydroxyl group (3,650–3,590 cm^{-1}), amine (3,500–3,300 cm^{-1}) and aromatic ring (3,050–3,000 cm^{-1}) containing drawn hydrogen are observed. This confirms the interaction of the effluent with the supported TiO_2 after the treatment. A characteristic peak of the CH_3 group is observed in the range of 2,400–2,300 cm^{-1}, while at 1,680–1,620 cm^{-1} the stretching of covalent C=C bonds of the aromatic ring is observed [36]. Peaks in frequency ranges of less than 1,000 cm^{-1} refer to stretches of metal interaction with TiO_2. At 700 cm^{-1} the M–OH stretcher peak was observed and at 550 cm^{-1} the O–Ti–O interaction, confirming that the catalyst remained in the aluminium support after treatment. Similar results can be found in the work of Santos et al. [37], which immobilized TiO_2 in polystyrene.

The SEM micrographs shown in Fig. 5 show the magnified surface at 20× for the aluminium support without calcination, with calcination and with calcination and immobilization of TiO_2.

It shows differences that the heat treatment made in the material, which became rough and uneven after calcination. The immobilized TiO_2 layer presented as a rough film (Fig. 5(c)) from TiO_2 agglomeration on the surface of the aluminum rings with subsequent thermal fixation. In the work of R. Ludwichk et al. [38], steel wires were covered with TiO_2 by thermal fixation, the rough surface of the support material is essential for the complete coating of its surface with the catalyst.

3.2. Preliminary tests

EI and EO effluents presented COD of 659.8 and 484.3 mg $O_2.L^{-1}$. Initially, tests were performed with EI and EO exposed to solar radiation. The results obtained of dyes and aromaticity removals are presented in Fig. 6. One can observe the effectiveness of each treatment over time.

As expected, direct photolysis did not show a significant decrease after 360 min of treatment. Organic pollutants, commonly present in textile effluents, have a complex structure and are hardly degradable with radiation alone [21], thus it is necessary to form reactive compounds such as HO· and O_2^{-}/·OOH in the system to obtain an effective degradation [48]. The Solar/H_2O_2 system did not present a good result, reaching a removal percentage less than 20% for aromaticity and slightly more for the dye removal after 360 min of treatment. In this case, the solar radiation was not enough to promote an efficient H_2O_2 cleavage into HO·, thus the application of hydrogen peroxide in combination with solar radiation was not effective to remove colour as observed in previous studies [49]. The solar/$TiO_{2suspended}$ system obtained higher removals, mainly dye removal in both effluents. The improvement with TiO_2 addition is related to the generation of reactive products such as HO·,O_2^{-} and HOO· [48]. The use of solar/$TiO_{2suspended}$/H_2O_2 reached a very high dye removal rate, achieving for both affluent almost 100% of removal. The aromaticity removal was lower, however it was in the vicinity of 60% and 80% in EI and EO, respectively. Although, that method presents satisfactory results, the use of suspended catalysts presents some disadvantages as the complicated process of its removal and high cost [50]. The efficiency of the photochemical process can also be reduced due to the high concentration of the photocatalyst, causing a poor distribution of the solar radiation, due to a high effluent turbidity [51,52]. The UV-solar/$TiO_{2supported}$/H_2O_2 system presented a slightly lower removal of aromaticity and dyes when compared with the UV-solar/$TiO_{2supported}$ system. That great efficiency resulted from the interaction of hydrogen peroxide

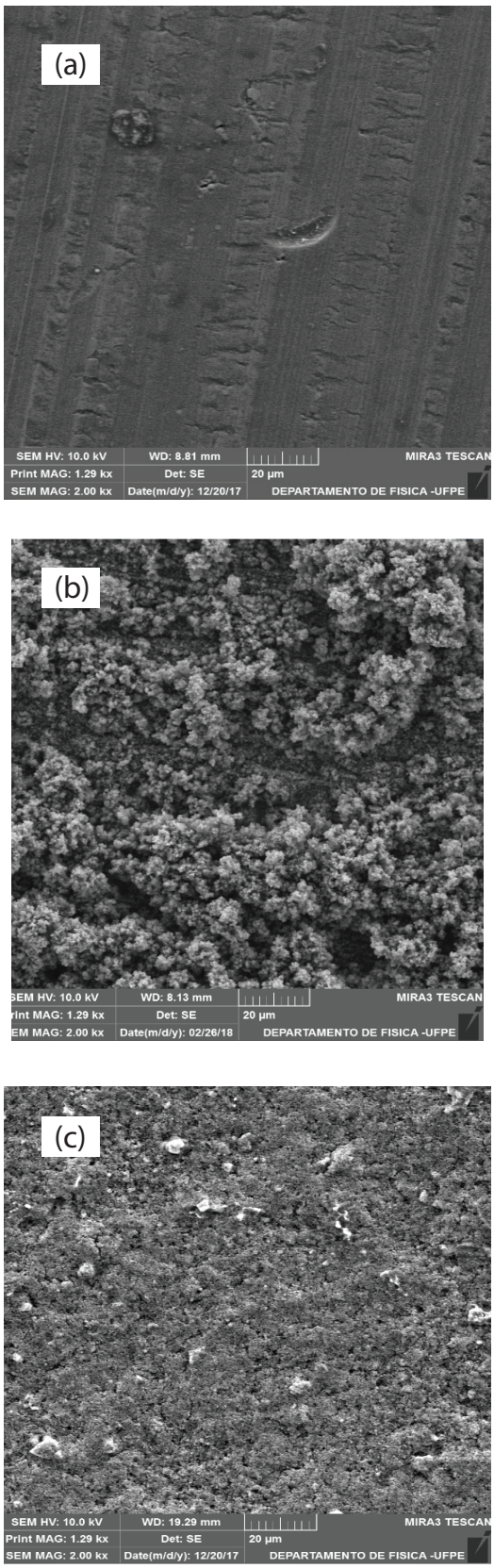

Fig. 5. SEM analysis of (a) aluminum bracket, (b) calcined aluminium bracket and (c) TiO_2 supported on aluminium mesh. Magnification of 100×.

and TiO_2, which increased the oxidative power due to higher HO·formation [48,53]. Although, supported TiO_2 presented lower removals than the supported system, it does not need the filtration step to remove the catalyst, thus making the system more applicable.

The same type of experiments was performed with the use of UV-C radiation. The results of aromaticity and dye removal of EI and EO are shown in Fig. 7.

The direct UV-C photolysis in both EI and EO effluent was more effective than direct solar photolysis. The low impact of solar radiation, which has about 5% of UV radiation, was expected since wavelengths and quantum yield are very low due to the less energetic bands [54]. The UV-C/$TiO_{2suspended}$ system showed very high dye removals, although the aromaticity removal was lower. It was expected that the use of TiO_2 in the UV-C system presented a higher percentage of degradation when compared with the Solar system since TiO_2 is able of absorbing only a small fraction of the solar radiation [51,52]. The UV-C/H_2O_2 system obtained also an expressive percentage of dye and aromaticity degradation than that obtained with solar radiation, reaching more than 60% in both cases. This result shows that solar radiation does not have enough energy to effectively break down H_2O_2 molecules, thus generating hydroxyl radicals [55]. The UV-C/$TiO_{2suspended}$ /H_2O_2 system due to the higher concentration of oxidant species was the most efficient system, presenting degradation higher than 80% for dye removal in both effluents. A lower aromaticity removal was obtained in the EI effluent. The UV-C/$TiO_{2supported}$ /H_2O_2 system presented a slightly lower result for degradation of the dyes and also when compared with the suspended system, which is similar to the solar systems.

3.3. Factorial planning for the solar/H_2O_2/$TiO_{2suported}$ system

The choice of EI to be used in the factorial planning was carried out by comparing the two effluents (EI and EO) after the applied treatments. The EI treated by the best system (Solar/TiO_2 /H_2O_2) obtained its highest percentage of degradation in 300 min of treatment, reaching 86% for aromatic compounds and 99% for dyes removal. The EO effluent had an aromaticity removal of 63% and 97% for the dyes removal when treated by (Solar /$TiO_{2suspended}$/H_2O_2). The choice of the Solar/TiO_2/H_2O_2 system was based on the degradation time for the EI effluent since it was the system that presented the highest aromaticity and dye removal. The economic benefits of using solar radiation have also been taken into account. The Pareto graph (Fig. 8) evaluated the statistical significance of the variables employed. The dating analysis was carried out using the Statistica 6.0 software.

The result of the statistical analysis indicates that the amount of H_2O_2 was the only variable with statistical significance in the degradation process. After the significance analysis, the highest concentration of hydrogen peroxide and lower TiO_2 dose were used in the recirculation reactor for the kinetic study.

3.4. Kinetics of textile effluent treatment by Solar/H_2O_2/$TiO_{2suported}$ in recirculation reactor

Considering the best treatment condition obtained through the factorial design, the experiment was repeated

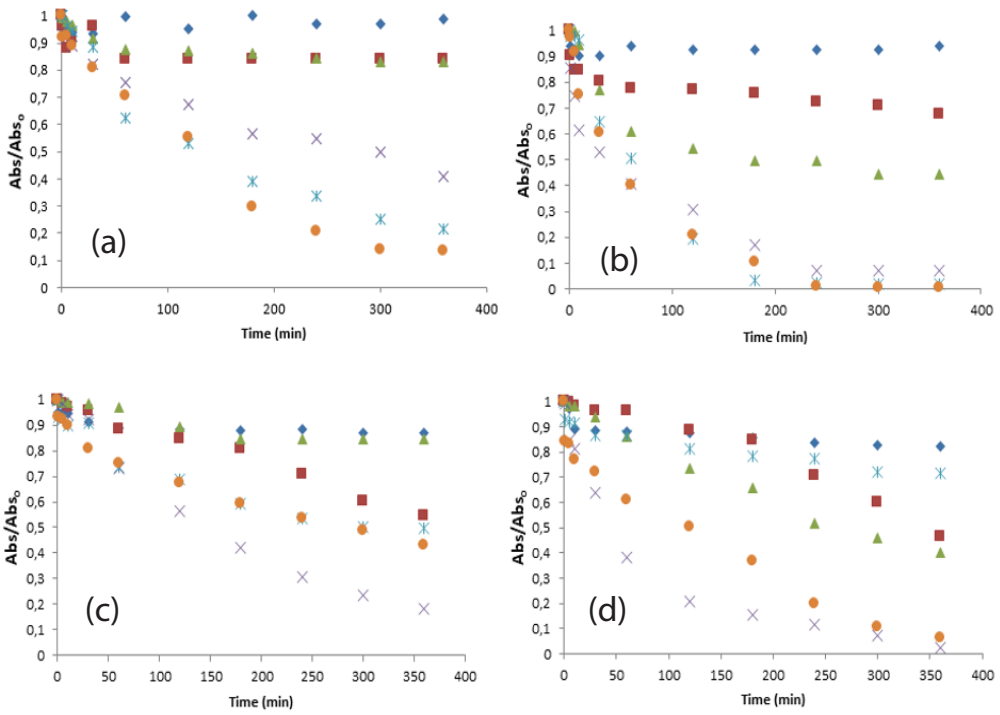

Fig. 6. Aromaticity and Dye removal from the EI and EO effluent using solar radiation: (a) aromaticity removal from EI; (b) dye removal from EI; (c) aromaticity removal from EO; and (d) dye removal from EO. ◊ = photolysis; □ = solar/H_2O_2; Δ = solar/$TiO_{2suspended}$; ○ = solar/$TiO_{2supported}$/H_2O_2; X = solar/$TiO_{2supported}$; x = solar/$TiO_{2suspended}$/H_2O_2.

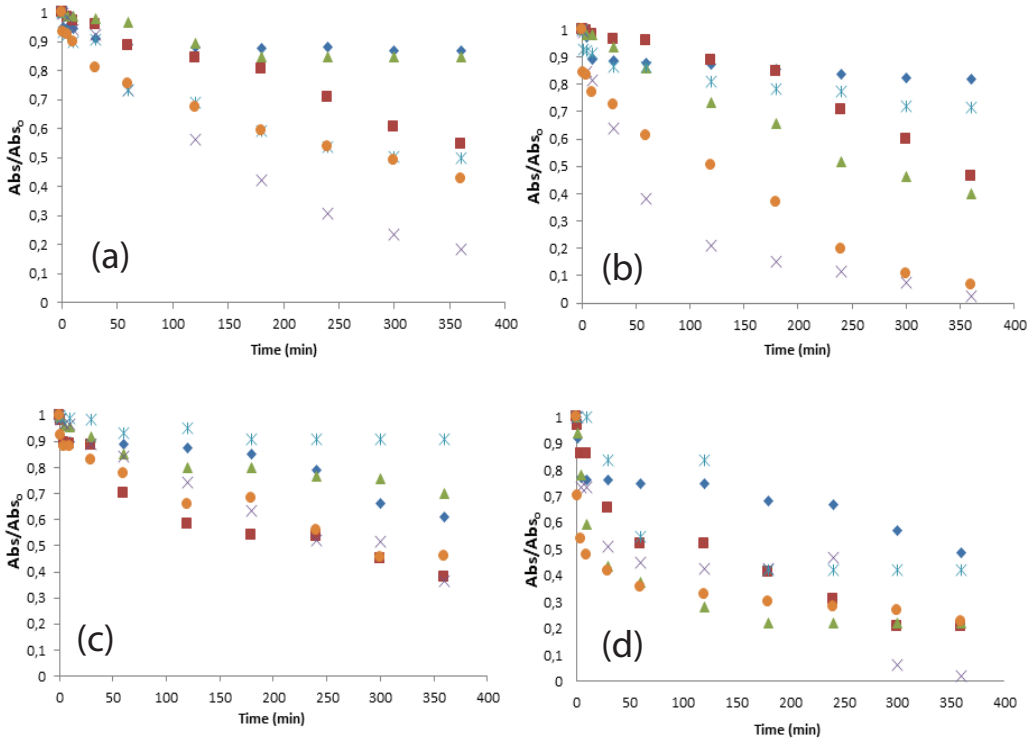

Fig. 7. Aromaticity and dye removal from the EI effluent using UV-C radiation: (a) aromaticity removal from EI; (b) dye removal from EI; (c) aromaticity removal from EO; and (d) dye removal from EO. ◊ = photolysis; □ = UV-C/H_2O_2; Δ = UV-C/$TiO_{2suspendeded}$; ○ = UV-C/$TiO_{2supported}$/H_2O_2; X = UV-C/$TiO_{2supported}$; x = UV-C/$TiO_{2suspended}$/H_2O_2.

in the recirculation reactor. Fig. 9 shows the aromaticity and dye removal throughout 360 min of treatment using the solar/H_2O_2/$TiO_{2suported}$ system.

According to the results, it was observed that there was a significant increase in the degradation percentage between 60 and 90 min, reaching about 30% for aromaticity and 61% for dye removals. High percentages of degradation were obtained after 240 min of treatment, which more than 90% degradation was achieved for the dyes. The obtained standard deviation was 0.06. From the degradation kinetics of dyes and aromatic compounds, the linear adjustments for the zero-order, pseudo-first order andsecond-order kinetic models were performed. The second order model described the degradation of both the dyes (r^2 = 0.9726) and the aromatics (r^2 = 0.8929). As expected, zero-order kinetics did not adequately describe the kinetics of the reaction, since the reaction encompasses complex mechanisms of radical formation, successive attacks of π-bonds on complex organic molecules, and transformation of organic carbon into the form of carbon dioxide [56]. According to Rosario-Ortiz et al. [57], second-order kinetics has been reported for many organic compounds, which are successively attacked during the POA process by the OH radicals formed.

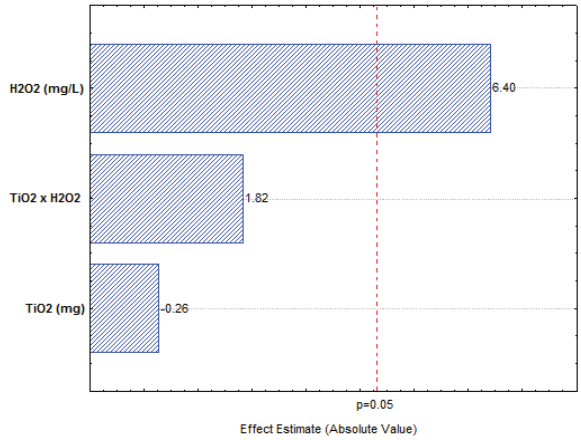

Fig. 8. Pareto chart for the 2^2 factorial design.

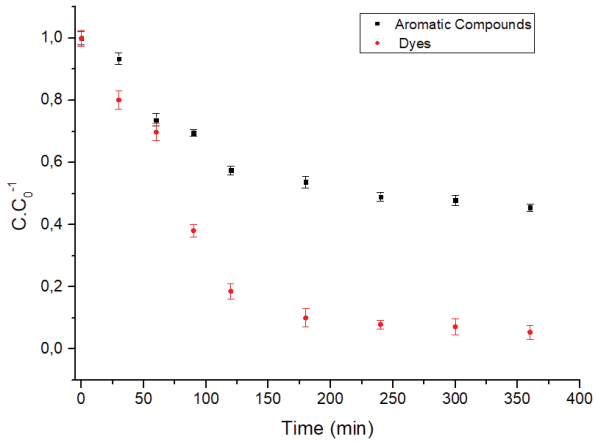

Fig. 9. Aromaticity and dye removal using solar/H_2O_2/TiO_2 during 360 min to dyes and aromatic compounds.

Based on the kinetic constant obtained for the second-order model k_{dye} = 0.175 L.mol^{-1}.s^{-1}, the sample half-life ($t_{1/2}$) was estimated from Eq. (3) to be 20.3 min.

$$t_{\frac{1}{2}} = \frac{1}{k.[\mathrm{Abs}(t=0)]} \quad (3)$$

Several studies have reported the isolated and combined use of H_2O_2 and TiO_2 for the degradation of textile effluents, as shown in Table 3.

Despite the long experimental time used in this study, the use of natural solar radiation eliminates the energy costs that would exist in other photocatalytic processes, with the use of UVC or mercury lamps. In addition, another important factor is that the system uses supported TiO_2, avoiding later steps of recovery of the photocatalyst. The recirculation system used in this work eliminated 95% of the colouration of the textile effluent and more than 70% COD, showing the efficiency of the combination of solar radiation, H_2O_2 and TiO_2.

3.5. Kinetic modelling through ANN

The training of simple ANN topology was tested and the result according to the mean absolute error was adopted for both solar/H_2O_2/$TiO_{2suported}$ for the aromaticity (254 nm) and dye (655 nm). A two-layer feed forward NN was adopted, with a sigmoid neuron-response function, and an independent (bias) term for the intermediate and output neuron layers, as described by Haikin [63]. To perform the ANN analysis the input and output values were normalized and

Table 3
Literature survey for the treatment of textile effluents by TiO_2 and H_2O_2

[H_2O_2] (mmol.L^{-1})	[TiO_2] (mg.L^{-1})	Radiation	Power (W)	% Color removal	% COD	Time	Reference
200	–	UV lamp	7.2	37	7	60	[58]
35	–	High-pressure	250	22.47	–	40	[59]
–	200	mercury lamp		36.28		120	
–	2,000	Mercury vapor lamp	125	88	20	360	[60]
–	500	Low-pressure mercury lamp	400	93	40	240	[61]
100	1,000	UV lamp	30	55	–	1,440	[62]
236	1,000	Solar light	–	95	75.6	360	This study

established between –1 and 1 for all set of data in order to guarantee the training to be reliable and rapid as exposed by Haikin [63].

ANN results of degradation data training for the effluent is presented in Fig. 10. In Fig. 10, the input layer (wavelength and time) and the output layer (representing the degradation response) are exhibited. The weights (values above the lines connecting the neurons) indicate the values which multiply the output values of a neuron before the value gets to next neuron, while the bias (the arrows pointing to the neurons) indicate the added values to the neuron inputs. This model is able to predict the degradation response for the effluent degradation under the given conditions.

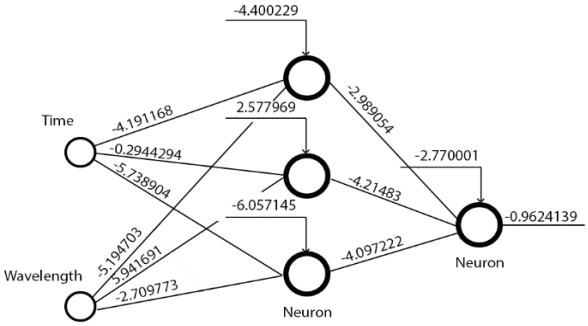

Fig. 10. ANN resulting from degradation data training by Solar/H_2O_2/$TiO_{2suported}$.

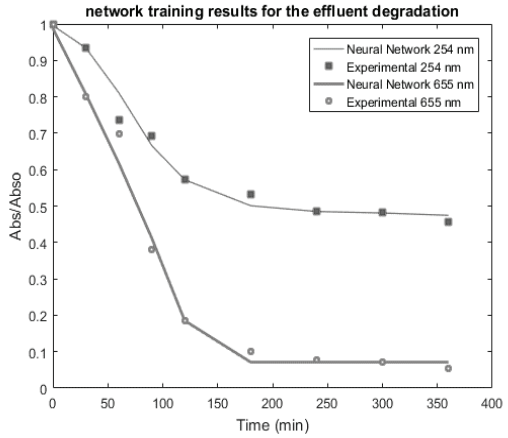

Fig. 11. Adjustment of the ANN model for Solar/H_2O_2/$TiO_{2suported}$.

Fig. 11 shows the adjustment of the training results to the experimental data in the Solar/H_2O_2/$TiO_{2suported}$.

According to the chart, a good prediction model could be achieved by the training with an absolute mean error estimated in 0.02266 after 9297552 interactions for photolysis, is possible to observe that ANN can detect subtle changes on experimental conditions, even if it is similar to experimental noise, but the point in 60 min in both wavelengths cannot be well predicted, since in Neural Networks the question of overfitting is always avoided, because the model need to generalize the data set.

3.6. Effluent characterization

The characterization of the textile effluents used in the present study was performed and it is presented in Table 4. The analyzed parameters were: pH, apparent color, conductivity, turbidity, total dissolved solids, nitrate and COD.

The obtained results for the effluents characterization before the photocatalytic treatment indicate the need for an alternative treatment to obtain better results before being discharged into water bodies. The other parameters, despite having suffered a reduction after the physical-chemical industrial treatments, did not present satisfactory values indicating that industrial (conventional) treatment is not efficient. With the application of the photocatalytic treatment, all the parameters suffered a reduction in their values. The COD decreased 75.6% in relation to the initial effluent and 66.7% in relation to the effluent after the conventional treatment of the industry. This result confirms the efficiency of the photocatalytic treatment in the treatment of effluents from the textile industry. The use of the reactor made of recycled material (PET) brings economic advantages, due to the low cost of obtaining the material and its respective construction. In addition, this reactor can be arranged in series for the treatment of a larger volume of effluent.

4. Conclusion

From the preliminary tests, using different processes of advanced oxidation, the most efficient degradation system for the aromatic compounds and dyes of the industrial effluent could be determined. The EI treatment by

Table 4
Effluent characterization

Parameters	EI	EO	Solar/H_2O_2/$TiO_{2suported}$ recirculation reactor
pH	7.4	7.4	9.0
Apparent color (mg $Pt.L^{-1}$)	385	200	48.8
Conductivity ($\mu s.cm^{-1}$)	11,220	9,620	9,970
Turbidity (NTU)	183	19.5	3.1
Total dissolved solids ($mg.L^{-1}$)	5,600	4,810	4,890
Nitrate ($mg.L^{-1}$)	0.9	0.9	0.5
COD (mg $O_2.L^{-1}$)	659.8	484.3	161.3

solar/$TiO_{2supported}$/H_2O_2 showed a higher percentage of degradation in a reasonable time of treatment. The high efficiency of the solar radiation when compared to the germicidal radiation presents several economic and environmental advantages, due to the abundance and gratuity of the solar radiation, leading to a decrease in energy costs and simplicity of the treatment. As expected, the combined TiO_2 and H_2O_2 were more efficient when compared with the other systems.

Through a factorial design, it was possible to find the best treatment conditions for this system, in order to reach higher percentages of degradation in shorter time intervals, with a lowercost. The performance of the experiment in the recirculation reactor allowed obtaining degradation kinetics by adjusting to a second order model. The use of artificial neural network was proven efficient to predict the degradation of a real effluent, resulted in mean absolute errors of 0.02266 for solar/H_2O_2/$TiO_{2suported}$, with the increasing application of machine learning, the use of the neural network in this paper show to be promising. With the results obtained in the present study, it was concluded that the treatment is suitable for the removal of contaminants from textile effluents presenting higher efficiency than the conventional treatment used in the industry under study.

The results presented in this new and cost-effective reactor can be scaled up and used to treat small volumes of textile wastewater, thus solving the problem of textile effluent treatment as well as use the fate of recyclable materials such as soda cans and PET bottles.

References

[1] A.R.A. Aziz, P. Asaithambi, W.M.A.B.W. Daud, Combination of electrocoagulation with advanced oxidation processes for the treatment of distillery industrial effluent, Process. Saf. Environ. Prot., 99 (2016) 227–235.

[2] M.A. Hassaan, A. El Nemr, F.F. Madkour, Advanced oxidation processes of Mordant Violet 40 dye in freshwater and seawater, Egypt. J. Aquat. Res., 43 (2017) 1–9.

[3] S.K. Sen, S. Raut, P. Bandyopadhyay, S. Raut, Fungal decolouration and degradation of azo dyes: a review, Fungal. Biol. Rev., 30 (2016) 112–133.

[4] O.R.S. da Rocha, R.F. Dantas, M.M.M.B. Duarte, M.M.L. Duarte, V.L. da Silva, Oil sludge treatment by photocatalysis applying black and white light, Chem. Eng. J., 157 (2010) 80–85.

[5] A.K. Verma, Treatment of textile wastewaters by electrocoagulation employing Fe-Al composite electrode, J. Water. Process. Eng., 20 (2017) 168–172.

[6] A. Kumar, P.V Nidheesh, M.S. Kumar, Composite wastewater treatment by aerated electrocoagulation and modified peroxi-coagulation processes, Chemosphere, 205 (2018) 587–593.

[7] T.W. Leal, L.A. Lourenço, A.S. Scheibe, S.M.A.G.U. De Souza, A.A.U. De Souza, Textile wastewater treatment using low-cost adsorbent aiming the water reuse in dyeing process, J. Environ. Chem. Eng., 6 (2018) 2705–2712.

[8] S. Wong, N. Atiqah, N. Yac, N. Ngadi, O. Hassan, I.M. Inuwa, From pollutant to solution of wastewater pollution: synthesis of activated carbon from textile sludge for dye adsorption, Chinese. J. Chem. Eng., 26 (2018) 870–878.

[9] A. Giwa, S. Chakraborty, M.O. Mavukkandy, H.A. Arafat, Nanoporous hollow fiber polyethersulfone membranes for the removal of residual contaminants from treated wastewater effluent : functional and molecular implications, Sep. Purif. Technol., 189 (2017) 20–31.

[10] J. Dasgupta, J. Sikder, S. Chakraborty, S. Curcio, E. Drioli, Remediation of textile effluents by membrane based treatment techniques: a state of the art review, J. Environ. Manage., 147 (2015) 55–72.

[11] G. Cinelli, F. Cuomo, L. Ambrosone, M. Colella, A. Ceglie, F. Venditti, F. Lopez, Photocatalytic degradation of a model textile dye using Carbon-doped titanium dioxide and visible light, J. Water. Process. Eng., 20 (2017) 71–77.

[12] A.D. Bokare, W. Choi, Review of iron-free Fenton-like systems for activating H_2O_2 in advanced oxidation processes, J. Hazard. Mater., 275 (2014) 121–135.

[13] A. Asghar, A.A.A. Raman, W.M.A.W. Daud, Advanced oxidation processes for in-situ production of hydrogen peroxide/hydroxyl radical for textile wastewater treatment: a review, J. Cleaner. Prod., 87 (2015) 826–838.

[14] M. Pourakbar, G. Moussavi, S. Shekoohiyan, Homogenous VUV advanced oxidation process for enhanced degradation and mineralization of antibiotics in contaminated water, Ecotoxicol. Environ. Saf., 125 (2016) 72–77.

[15] O. Rozas, C. Vidal, C. Baeza, W.F. Jardim, A. Rossner, H.D. Mansilla, Organic micropollutants (OMPs) in natural waters: oxidation by UV/H_2O_2 treatment and toxicity assessment, Water. Res., 98 (2016) 109–118.

[16] M.P. Rayaroth, U.K. Aravind, C.T. Aravindakumar, Sonochemical degradation of Coomassie Brilliant Blue: effect of frequency, power density, pH and various additives, Chemosphere, 119 (2015) 848–855.

[17] M. Bagheri, M. Mohseni, Impact of hydrodynamics on pollutant degradation and energy efficiency of VUV/UV and H_2O_2/UV oxidation processes, J. Environ. Manage., 164 (2015) 114–120.

[18] S. Marmitt, L.V. Pirotta, S. Stülp, Aplicação de fotólise direta e UV/H_2O_2 a efluente sintético contendo diferentes corantes alimentícios (in Portuguese), Quim. Nova., 33 (2010) 384–388.

[19] L.A.V. de Luna, T.H.G. da Silva, R.F.P. Nogueira, F. Kummrow, G.A. Umbuzeiro, Aquatic toxicity of dyes before and after photo-Fenton treatment, J. Hazard. Mater., 276 (2014) 332–338.

[20] A. Adak, K.P. Mangalgiri, J. Lee, L. Blaney, UV irradiation and UV-H_2O_2 advanced oxidation of the roxarsone and nitarsone organoarsenicals, Water. Res., 70 (2015) 74–85.

[21] R.P. Cavalcante, R.F. Dantas, B. Bayarri, O. González, J. Giménez, S. Esplugas, A. Machulek, Photocatalytic mechanism of metoprolol oxidation by photocatalysts TiO_2 and TiO_2 doped with 5% B: primary active species and intermediates, Appl. Catal. B. Environ., 194 (2016) 111–122.

[22] H. Dai, Y. Sun, P. Ni, W. Lu, S. Jiang, Y. Wang, Z. Li, Z. Li, Three-dimensional TiO_2 supported silver nanoparticles as sensitive and UV-cleanable substrate for surface enhanced Raman scattering, Sensor. Actuat. B. Chem., 242 (2017) 260–268.

[23] Y. Wang, S. Zhang, Y. Zeng, M. Ou, Q. Zhong, Photocatalytic oxidation of NO over TiO_2-Graphene catalyst by UV/H_2O_2 process and enhanced mechanism analysis, J. Mol. Catal. A: Chem., 423 (2016) 339–346.

[24] R. Willumeit, F. Feyerabend, N. Huber, Magnesium degradation as determined by artificial neural networks, Acta. Biomater., 9 (2013) 8722–8729.

[25] L. Das, U. Maity, J.K. Basu, The photocatalytic degradation of carbamazepine and prediction by artificial neural networks, Process. Saf. Environ. Prot., 92 (2013) 888–895.

[26] D.S. De Sá, L.E. Vasconcellos, J.R. De Souza, B.A. Marinkovic, T. Del Rosso, D. Fulvio, Intensification of photocatalytic degradation of organic dyes and phenol by scale-up and numbering-up of meso- and micro fluidic TiO_2 reactors for wastewater treatment, J. Photochem. Photobiol. A. Chem., 364 (2018) 59–75.

[27] D.D. Phan, T.H.T. Trinh, F. Babick, M.T. Nguyen, W. Samhaber, M. Stintz, Investigation of fixed-bed photocatalytic membrane reactors based on submerged ceramic membranes, Chem. Eng. Sci., 191 (2018) 332–342.

[28] M.E. Leblebici, G.D. Stefanidis, T. Van Gerven, Comparison of photocatalytic space-time yields of 12 reactor designs for wastewater treatment, Chem. Eng. Process. Process. Intensif., 97 (2015) 106–111.

[29] H. Amiri, B. Ayati, H. Ganjidoust, Mass transfer phenomenon in photocatalytic cascade disc reactor: effects of artificial roughness and flow rate, Chem. Eng. Process. Process. Intensif., 116 (2017) 48–59.

[30] C.B. Ozkal, Z. Frontistis, M. Antonopoulou, I. Konstantinou, D. Mantzavinos, S. Meriç, Removal of antibiotics in a parallel-plate thin-film-photocatalytic reactor: process modeling and evolution of transformation by-products and toxicity, J. Environ. Sci. (China)., 60 (2016) 114–122.
[31] K.O. Hamaloglu, E. Sag, A. Tuncel, Bare, gold and silver nanoparticle decorated, monodisperse-porous titania microbeads for photocatalytic dye degradation in a newly constructed microfluidic, photocatalytic packed-bed reactor, J. Photochem. Photobiol. A., 332 (2017) 60–65.
[32] A. Matilainen, M. Sillanpää, Removal of natural organic matter from drinking water by advanced oxidation processes, Chemosphere, 80 (2010) 351–365.
[33] P.R. Gogate, A.B. Pandit, A review of imperative technologies for wastewater treatment I: oxidation technologies at ambient conditions, Adv. Environ. Res., 8 (2004) 501–551.
[34] S. Mozia, Photocatalytic membrane reactors (PMRs) in water and wastewater treatment. A review, Sep. Purif. Technol., 73 (2010) 71–91.
[35] H. Zangeneh, A.A.L. Zinatizadeh, M. Habibi, M. Akia, M. Hasnain Isa, Photocatalytic oxidation of organic dyes and pollutants in wastewater using different modified titanium dioxides: a comparative review, J. Ind. Eng. Chem., 26 (2015) 1–36.
[36] F. Magalhães, R.M. Lago, Floating photocatalysts based on TiO_2 grafted on expanded polystyrene beads for the solar degradation of dyes, Sol. Energy., 83 (2009) 1521–1526.
[37] A.L. De Barros, A.A.Q. Domingos, P.B.A. Fechine, D. De Keukeleire, R.F. Do Nascimento, PET as a support material for TiO_2 in advanced oxidation processes, J. Appl. Polym. Sci., 131 (2014) 1–9.
[38] R. Ludwichk, O.K. Helferich, C.P. Kist, A.C. Lopes, T. Cavasotto, D.C. Silva, M. Barreto-Rodrigues, Characterization and photocatalytic treatability of red water from Brazilian TNT industry, J. Hazard. Mater., 293 (2015) 81–86.
[39] B. Erjavec, P. Hudoklin, K. Perc, T. Tišler, M.S. Dolenc, A. Pintar, Glass fiber-supported TiO_2 photocatalyst: efficient mineralization and removal of toxicity/estrogenicity of bisphenol A and its analogs, Appl. Catal. B., 183 (2016) 149–158.
[40] E. Topkaya, M. Konyar, H.C. Yatmaz, K. Öztürk, Pure ZnO and composite ZnO/TiO_2 catalyst plates: a comparative study for the degradation of azo dye, pesticide and antibiotic in aqueous solutions, J. Colloid Interface Sci., 430 (2014) 6–11.
[41] S.C. Lenore, E.G. Arnold, D.E. Andrew, Standard Methods for the Examination of Water and Wastewater, 20th, New York, 1998.
[42] L. Wood, D.L. Tauc, Weak absorption tails in amorphous semiconductors, Phys. Rewiew. B., 5 (1972) 3144.
[43] W.J. Do Nascimento Júnior, O.R.S. da Rocha, R.F. Dantas, J.P. da Silva, A.A. Barbosa, Kinetic study of food dyes removal from aqueous solutions by solar heterogeneous photocatalysis with artificial neural networks and phytotoxicity assessment, Desal. Wat. Treat., 104 (2018) 304–314.
[44] J. Matos, A. García, L. Zhao, M. Magdalena, Solvothermal carbon-doped TiO_2 photocatalyst for the enhanced methylene blue degradation under visible light, Appl Catal. A., 390 (2010) 175–182.
[45] S. Go, E. Oliveros, S.H. Bossmann, R. Guardani, C.A.O. Nascimento, Modeling the kinetics of a photochemical water treatment process by means of artificial neural networks, Chem. Eng. Process., 38 (1999) 373–382.
[46] J.A. Giroto, R. Guardani, A.C.S.C. Teixeira, C.A.O. Nascimento, Study on the photo-Fenton degradation of polyvinyl alcohol in aqueous solution, Chem. Eng. Process., 45 (2006) 523–532.
[47] R. Kennedy, J; Eberhart, Particle swarm optimization, in: IEEE Int. Conf., 1995.
[48] D. Wiedmer, E. Sagstuen, K. Welch, H.J. Haugen, H. Tiainen, Oxidative power of aqueous non-irradiated TiO_2-H_2O_2 suspensions: methylene blue degradation and the role of reactive oxygen species, Appl. Catal. B. Environ., 198 (2016) 9–15.
[49] V.J.P. Vilar, L.X. Pinho, A.M.A. Pintor, R.A.R. Boaventura, Treatment of textile wastewaters by solar-driven advanced oxidation processes, Sol. Energy., 85 (2011) 1927–1934.
[50] Z.A.M. Hir, P. Moradihamedani, A.H. Abdullah, M.A. Mohamed, Immobilization of TiO_2 into polyethersulfone matrix as hybrid film photocatalyst for effective degradation of methyl orange dye, Mater. Sci. Semicond. Process., 57 (2017) 157–165.
[51] M.E. Borges, M. Sierra, E. Cuevas, R.D. García, P. Esparza, Photocatalysis with solar energy: sunlight-responsive photocatalyst based on TiO_2 loaded on a natural material for wastewater treatment, Sol. Energy., 135 (2016) 527–535.
[52] M.E. Borges, M. Sierra, J. Méndez-Ramos, P. Acosta-Mora, J.C. Ruiz-Morales, P. Esparza, Solar degradation of contaminants in water: TiO_2 solar photocatalysis assisted by up-conversion luminescent materials, Sol. Energy. Mater. Sol. Cells., 155 (2016) 194–201.
[53] M.J. Abeledo-Lameiro, A. Reboredo-Fernández, M.I. Polo-López, P. Fernández-Ibáñez, E. Ares-Mazás, H. Gómez-Couso, Photocatalytic inactivation of the waterborne protozoan parasite Cryptosporidium parvum using TiO_2/H_2O_2 under simulated and natural solar conditions, Catal. Today., 280 (2017) 132–138.
[54] S. Giannakis, F.A. Gamarra Vives, D. Grandjean, A. Magnet, L.F. De Alencastro, C. Pulgarin, Effect of advanced oxidation processes on the micropollutants and the effluent organic matter contained in municipal wastewater previously treated by three different secondary methods, Water. Res., 84 (2015) 295–306.
[55] I. Velo-Gala, J.A. Pirán-Montaño, J. Rivera-Utrilla, M. Sánchez-Polo, A.J. Mota, Advanced Oxidation Processes based on the use of UVC and simulated solar radiation to remove the antibiotic tinidazole from water, Chem. Eng. J., 323 (2017) 605–617.
[56] J. Ma, M. Yang, F. Yu, J. Zheng, Water-enhanced Removal of Ciprofloxacin from Water by Porous Graphene Hydrogel, Sci. Rep., 5 (2015) 1–10.
[57] F.L. Rosario-Ortiz, E.C. Wert, S.A. Snyder, Evaluation of UV/H_2O_2 treatment for the oxidation of pharmaceuticals in wastewater, Water. Res., 44 (2010) 1440–1448.
[58] L. Bilińska, M. Gmurek, S. Ledakowicz, Comparison between industrial and simulated textile wastewater treatment by AOPs – Biodegradability, toxicity and cost assessment, Chem. Eng. J., 306 (2016) 550–559.
[59] M.S. Kumar, S.H. Sonawane, B.A. Bhanvase, B. Bethi, Treatment of ternary dye wastewater by hydrodynamic cavitation combined with other advanced oxidation processes (AOP's), J. Water Process. Eng., 23 (2018) 250–256.
[60] G.S. Arcanjo, A.H. Mounteer, C.R. Bellato, L.M.M. da Silva, S.H. Brant Dias, P.R. da Silva, Heterogeneous photocatalysis using TiO_2 modified with hydrotalcite and iron oxide under UV–visible irradiation for color and toxicity reduction in secondary textile mill effluent, J. Environ. Manage., 211 (2018) 154–163.
[61] P.A. Pekakis, N.P. Xekoukoulotakis, D. Mantzavinos, Treatment of textile dyehouse wastewater by TiO_2 photocatalysis, Water. Res., 40 (2006) 1276–1286.
[62] A. Touati, T. Hammedi, W. Najjar, Z. Ksibi, S. Sayadi, Photocatalytic degradation of textile wastewater in presence of hydrogen peroxide: effect of cerium doping titania, J. Ind. Eng. Chem., 35 (2016) 36–44.
[63] S. Haikin, Neural Networks: A Comprehensive Foundation, second, Prentice Hall, Upper Saddle River, 1999.